Supporting information

This supplementary includes the following supporting information:

Supplementary Methods: Detailed description of dissolved organic carbon and dissolved oxygen flux calculations.

Supplementary Discussion: Discussion about the incubation of extracellular enzyme samples under N_2 atmosphere.

Supplementary Figure 1: Extracellular enzyme rates with all samples incubated under N_2 atmosphere irrespective of the *in situ* oxygen concentration.

Supplementary Table 1: Cruise, date, positions, sampled depths and bottom depth of all stations represented within the manuscript.

Supplementary Table 2: Average and standard deviation at different oxygen regimes of all discussed parameters.

Supplementary Methods:

Diapycnal fluxes of oxygen and dissolved organic carbon

The mixing of DOC and oxygen across density surfaces is derived following Fischer et al. (2013) and Schafstall et al. (2010). Gradients of DOC where calculated between sampled bottles assuming a constant gradient in between while oxygen gradients were derived by fitting a linear trend over 3 m intervals, as oxygen is available on a much higher vertical resolution of 1dbar.

The diapycnal flux of solutes, i.e. DOC and oxygen, is calculated as

$$\Phi_S = -K_\rho \nabla C_S$$

Where $\nabla C_S$is the vertical gradient of the solute – in case of oxygen the concretion is converted from µmol kg^{-1} to µmol m^{-3} beforehand – and K_ρ is the diapycnal diffusivity of mass. We assume K_ρ to be equal to the diffusivity of DOC and oxygen, i.e. $K_\rho = K_{DOC} = K_{DO}$ as done by Fischer et al. (2013) for oxygen.

The diapycnal diffusivity is calculated following Osborn (1980):

$$K_\rho = \Gamma \frac{\varepsilon}{N^2}$$

Where $\Gamma = 0.2$ is the mixing efficiency, ε (m^2 s^{-3}) is the dissipation rate of turbulent kinetic energy calculated by integrating the shear spectra derived from measurements on a freefalling microstructure probe at stations G-N & Q-T (Sea & Sun Technology, MSS90D, S/N26 up to CTD 43, S/N 73 afterwards) (Schafstall et al., 2010), and N (s^{-1}) is the buoyancy frequency derived from CTD downcast profiles over 7 dbar intervals where DOC and oxygen were measured as well.

To calculate K_ρ, data from CTD profiles we combined with nearby microstructure profiles conducted directly before or after the CTD profile which existed for 12 profile. For each solutes gradient between to samples a $K_\rho$value was derived from dissipation and buoyancy frequency averaged between the potential densities of the two solutes samples. The mean K_ρ profile exhibits only weak vertical variations (Supplementary Figure 2a) therefore a constant $K_\rho = 10^{-3} m^2 s^{-1}$ was used to calculate fluxes.

For each profile a Φ_S profile is calculated in 20 m depth bins, from these a mean profile of diapycnal flux is derived. Subsequent, the vertical divergence of the mean flux profile of DOC or oxygen is given by $\nabla \Phi_S = -\frac{\partial}{\partial z}\Phi_S$.

The error estimates of these terms are calculated following Schafstall et al. (2010), with the error of the mean $K_\rho$given by:

$$\Delta K_\rho = K_\rho \left[\left(\frac{\Delta \Gamma}{\Gamma}\right)^2 + \left(\frac{\Delta \varepsilon}{\varepsilon}\right)^2 + \left(\frac{\Delta N^2}{N^2}\right) \right]^{\frac{1}{2}}$$

And the error of the mean flux by

$$\Delta\Phi_S = \Phi_S \left[\left(\frac{\Delta\Gamma}{\Gamma}\right)^2 + \left(\frac{\Delta\varepsilon}{\varepsilon}\right)^2 + \left(\frac{\Delta N^2}{N^2}\right) + \left(\frac{\Delta\nabla C_S}{\nabla C_S}\right) \right]^{\frac{1}{2}}$$

Where K_ρ and Φ_S are the mean profiles calculated from the individual profiles in 20 m depth bins, a constant $\Delta\Gamma = 0.04$ is used (Schafstall et al., 2010), the error of dissipation $\Delta\varepsilon$is the 95%-confidence interval derived by bootstrapping, $\Delta N^2$and $\Delta\nabla C_S$are the standard deviations of the mean. Bootstrapping and standard deviations are performed on the values of the individual profiles in 20 m bins. The error of the change in the diapycnal flux over depth is derived by error propagation from the flux.

Supplementary Discussion:

Incubation of extracellular enzyme samples under N_2 atmosphere

Enzyme rates of suboxic waters have been obtained by incubating samples under N_2 atmosphere to reduce oxygen concentrations. For the assessment of extracellular enzyme rates we chose to incubate samples at oxic and reduced oxygen concentrations depending on oxygen concentrations at *in situ* depth (see methods for details). Incubation conditions slightly influenced the resulting enzyme rates. Incubating samples from depths with *in situ* oxygen concentrations <5 µmol kg^{-1} under N_2 atmosphere, instead of under atmospheric oxygen concentrations, yielded on average 2-27% higher rates. Consequently, the differences in rates between oxic and suboxic waters became reduced, when all samples were incubated under N_2 atmosphere (supplementary Figure 2). However, the observed trends over depth remained similar. Possible reasons for higher extracellular enzyme rates after incubation under N_2 atmosphere are changes in (i) pH, (ii) the abundance of oxygen radicals and/or (iii) changes in enzyme production. (i) Higher extracellular enzyme rates after incubations at low oxygen concentrations are less likely driven by the resulting increase in pH (Δ 0.4), since earlier studies rather suggested that extracellular enzyme rates decrease with pH (Endres et al., 2014; Piontek et al., 2013). (ii) Oxygen radicals can destroy enzymes (Elstner, 1990). Since our incubations were not completely anoxic, an influence of oxygen radicals on enzyme activity cannot be excluded, but would appear under aerobic and N_2 atmosphere. (iii) Finally, an enhanced production of enzymes within the 12 hours of incubation time might be the reason for higher rates after incubations under N_2 atmosphere. It has been shown before that enzymes can be produced within 30 minutes (Both et al., 1972), making this explanation likely. The final reason for higher enzyme productions under N_2 atmosphere remains a matter of speculation, but supports the trends seen in the depth profiles and does not restrict the interpretation of the extracellular enzyme data.

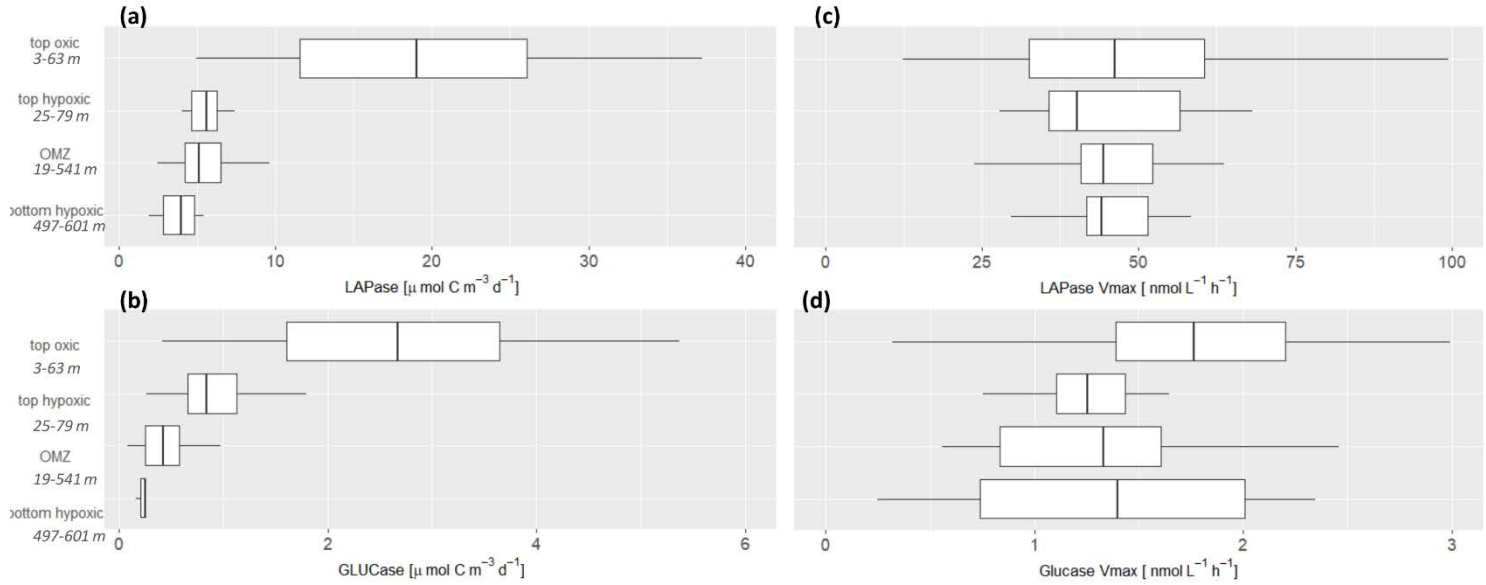

Supplementary Figure 1: Extracellular enzyme rates with all samples incubated under N_2 atmosphere irrespective of the *in situ* oxygen concentration. Degradation rates of dissolved amino acids (DHAA) by leucine-aminopeptidase (LAPase) **(a)**, degradation rates of high molecular weight dissolved carbohydrates (DCHO) by ß-glucosidase (GLUCase) **(b)** total potential LAPase rates (V_{max}) **(c)**, Glucase V_{max} **(d)** at different oxygen regimes.

Supplentary Table 1: Cruise, date, positions, sampled depths and bottom depth of all stations represented within the manuscript. Extracellular enzyme rates were sampled at stations A-K, whereas some depths were not used for further analyses, since the standard deviation was over 30%. Bacterial biomass production was sampled at stations G-T. Stations G-T were included in the estimation of carbon and oxygen loss rates. Cell abundance was sampled at every station.

Cruise	Station	Latitude	Longitude	Date	Sampled Depth						Bottom Depth
M138	A	-15.5393	-75.6149	06/19/2017	3	17	24	28	39		2507
					99	197	396	596	1499		
M138	B	-15.8595	-76.1099	06/21/2017	5	18	40	50	53		2624
					90	199	398	600			
M138	C	-16.1593	-76.5711	06/21/2017	3	13	19	58	63		3679
					79	99	149	197	347	600	
M138	D	-13.9971	-76.6598	06/16/2017	3	8	19	48	70		586
					98	117	197	397	498	541	
M138	E	-14.2988	-77.1796	06/17/2017	19	38	47	66	97		4702
					147	198	299	398	497	601	
M138	F	-14.7596	-77.4829	06/23/2017	9	28	48	53	99		4154
					148	197	297	397	497	601	
M136	G	-12.2248	-77.1795	04/27/2017	4	20	25	30	39		75
					49	59	72				
M136	H	-12.3584	-77.3621	04/25/2017	3	6	27	39	48		194
					58	68	79	98	128		
M136	I	-12.453	-77.4918	04/26/2017	4	18	28	39	49		403
					59	73	199				
M136	J	-12.5807	-77.6731	04/29/2017	4	28	49	68	78		973
					99	195	393	448	498	598	
M136	K	-12.338	-78.0512	04/26/2017	9	50	75	99	148		1970
					157	199	299	398	499	599	
M136	L	-12.2782	-77.2493	04/20/2017	4	9	13	19	23		130
					28	43	48	58			
M136	M	-12.5806	-77.6731	04/19/2017	3	19	39	55	65		242
					90	98	199	238			
M136	N	-12.4134	-77.4425	04/21/2017	3	18	50	99	124		307
					149	174	224	272	300		
M136	O	-12.5226	-77.5834	04/20/2017	4	29	39	49	59		751
					79	89	98	147	597	745	
M136	P	-12.9873	-78.2471	04/21/2017	4	29	49	60	74		5410
					99	196	296	396	599	800	
M136	Q	-13.8938	-76.5101	04.12.2017	4	10	15	19	30		166
					39	50	69	99	128	159	
M136	R	-14.1878	-76.9312	04/13/2017	5	14	29	49	81		3042
					101	123	199	399	599		
M136	S	-14.3986	-77.2389	04/14/2017	1	49	89	99	148		5149
					198	299	399	499	599		
M136	T	-12.2254	-77.1797	04/24/2017	4	19	24	28	49		76

Supplementary Table 2: Average and standard deviation at different oxygen regimes of all discussed parameters as total rates **(a)** and cell-specific rates **(b)**.

a						
parameter	**station**	**oxygen regime**	**n**	**mean**	**SD**	**unit**
cell abundance	A-T	top oxic top high hypoxic top low hypoxic OMZ bottom low hypoxic top oxycline	52 16 20 93 14 36	19 9 8 9 1 9	9 3 3 5 0.1 3	cells x 10^5 mL^{-1}
bacterial production	G-T	top oxic top high hypoxic top low hypoxic OMZ bottom low hypoxic oxycline	34 11 17 48 5 33	194 58 43 26 5 42	189 61 38 32 3 47	µmol C m^{-3} d^{-1}
degradation rates of DHAA by LAPase	A-K	top oxic top high hypoxic top low hypoxic OMZ bottom low hypoxic	20 6 9 41 6	13.9 4.5 2.4 5.0 2.4	7.6 3.0 1.2 1.8 1.6	µmol C m^{-3} d^{-1}
degradation rates of DCHO by GLUCase	A-K	top oxic top high hypoxic top low hypoxic OMZ bottom low hypoxic	22 7 8 35 3	2.7 1.5 0.8 0.7 0.4	2.5 1.0 0.5 1.4 0.3	µmol C m-3 d-1
LAPase Vmax	A-K	top oxic top high hypoxic top low hypoxic OMZ bottom low hypoxic	22 10 10 49 6	39.2 41.1 28.9 49.9 31.3	13.3 24.0 13.6 22.1 6.0	nmol L^{-1} h^{-1}
GLUCase Vmax	A-K	top oxic top high hypoxic top low hypoxic OMZ bottom low hypoxic	26 9 11 41 4	1.6 1.4 1.0 1.6 0.7	0.6 0.5 0.3 1.6 0.4	nmol L^{-1} h^{-1}

b						
parameter	**station**	**oxygen regime**	**n**	**mean**	**SD**	**unit**
cell-specific bacterial productio	G-T	top oxic top high hypoxic top low hypoxic OMZ bottom low hypoxic oxycline	34 11 17 48 5 33	92 50 46 22 35 45	78 36 27 19 23 29	amol C cell d^{-1}
cell-specific Degradation rates of DHAA by LAPase	A-K	top oxic top high hypoxic top low hypoxic OMZ bottom low hypoxic	20 6 9 41 6	6.5 4.6 3.1 9.9 21.6	3.4 3.1 1.6 6.8 15.4	amol C cell d^{-1}
cell-specific Degradation rates of DCHO by GLUCase	A-K	top oxic top high hypoxic top low hypoxic OMZ bottom low hypoxic	22 7 8 35 3	1.3 1.4 1.1 1.1 3.2	1.6 1.1 0.8 1.6 3.2	amol C cell d^{-1}
cell-specific LAPase Vmax	A-K	top oxic top high hypoxic top low hypoxic OMZ bottom low hypoxic	22 10 10 49 6	23.1 44.1 39.9 103.5 274.1	15.1 29.7 23.0 114.2 51.7	amol $cell^{-1}$ h^{-1}
cells-specific GLUCase Vmax	A-K	top oxic top high hypoxic top low hypoxic OMZ bottom low hypoxic	26 9 11 41 4	0.9 1.5 1.3 2.7 6.0	0.4 0.6 0.5 2.4 3.6	amol $cell^{-1}$ h^{-1}

References_supplement

Both, G. W., McInnes, J. L., Hanlon, J. E., May, B. K. and Elliott, W. H.: Evidence for an accumulation of messenger RNA specific for extracellular protease and its relevance to the mechanism of enzyme secretion in bacteria, J. Mol. Biol., 67(2), 199–217, doi:10.1016/0022-2836(72)90236-7, 1972.

Elstner, E. F., Ed.: Der Sauerstoff: Biochemie, Biologie, Medizin, BI-Wiss_Verl, Mannheim., 1990.

Endres, S., Galgani, L., Riebesell, U., Schulz, K.-G. and Engel, A.: Stimulated Bacterial Growth under Elevated pCO2: Results from an Off-Shore Mesocosm Study, edited by S. Dupont, PLoS One, 9(6), e99228, doi:10.1371/journal.pone.0099228, 2014.

Fischer, T., Banyte, D., Brandt, P., Dengler, M., Krahmann, G., Tanhua, T. and Visbeck, M.: Diapycnal oxygen supply to the tropical North Atlantic oxygen minimum zone, Biogeosciences, 10(7), 5079–5093, doi:10.5194/bg-10-5079-2013, 2013.

Osborn, T. R.: Estimates of the local rate of vertical diffusion from dissipation measurements, J. Phys. Oceanogr., 10(1), 83–89, doi:10.1175/1520-0485(1980)010<0083:EOTLRO>2.0.CO;2, 1980.

Piontek, J., Borchard, C., Sperling, M., Schulz, K. G., Riebesell, U. and Engel, A.: Response of bacterioplankton activity in an Arctic fjord system to elevated pCO_2: results from a mesocosm perturbation study, Biogeosciences, 10(1), 297–314, doi:10.5194/bg-10-297-2013, 2013.

Schafstall, J., Dengler, M., Brandt, P. and Bange, H.: Tidal-induced mixing and diapycnal nutrient fluxes in the Mauritanian upwelling region, J. Geophys. Res., 115(C10), C10014, doi:10.1029/2009JC005940, 2010.